Eur. Phys. J. D **11**, 109–114 (2000)

THE EUROPEAN PHYSICAL JOURNAL D

EDP Sciences

The internal energy of small ammonia clusters in a supersonic beam and after scattering off LiF(100)

C. Menzel[a] and H. Zacharias[b]

Physikalisches Institut, Westfälische Wilhelms-Universität, 48149 Münster, Germany

Received 18 October 1999 and Received in final form 10 December 1999

Abstract. The photoionization efficiency (PIE) of neutral ammonia clusters is studied as a function of photon energy. From these curves the internal energies of clusters in the incident supersonic beam and of clusters surviving after scattering off a LiF(100) surface are derived. A supersonic expansion of ammonia seeded in He produces small clusters of various size but with uniform kinetic energy of about 285 meV per monomer molecule. The mass distribution of clusters in the jet and of the scattered particles is measured in a reflecting time-of-flight mass spectrometer by single photon photoionization using vacuum ultraviolet (VUV) laser radiation tunable between $\lambda = 142.5$ nm ($h\nu = 8.7$ eV) and $\lambda = 126.5$ nm ($h\nu = 9.8$ eV). In the incident beam the internal energies of clusters up to $n = 15$ do not vary significantly and amount to an average of about (65 ± 3) meV. After scattering off LiF(100) the internal energy of clusters up to $n = 4$ increases with fragment size and amounts to about half a monomer binding energy.

PACS. 36.40.Sx Diffusion and dynamics of clusters – 68.45.Da Adsorption and desorption kinetics; evaporation and condensation – 82.65.Pa Surface-enhanced molecular states and other gas-surface interactions

1 Introduction

The collisional dynamics of the interaction of neutral clusters with single crystal surfaces has attracted considerable interest in recent years. The unique feature of this scattering event is the rapid redistribution of kinetic energy over many constituents and degrees of freedom. Experimental investigations have mostly been performed for weakly bound van der Waals clusters [1–3] and a few for more tightly bound hydrogen-bonded clusters like ammonia [4,5], water [6–8] and ethanol [9]. The total kinetic energy even of comparatively slow neutral clusters in a molecular beam is significantly higher than the binding energy of individual constituents. The energy redistribution then leads to a break-up of the cluster into mostly small fragments. Insight into the dynamics may be gained from measurements of the angular, velocity and internal energy distributions of scattered fragments and a comparison with theoretical model calculations. Molecular dynamics simulations have been carried out for the scattering of small and large rare gas [10–14] and water [15] clusters. A thermokinetic model has been proposed by Vach *et al.* [3,16], which describes the observed angular and velocity distributions of monomers from weakly bound clusters quite well. These distributions differ considerably from those known in monomer scattering. The kinetic energy distribution of monomers evaporated from large rare gas clusters is often close to Maxwellian at the critical temperature of the species. For hydrogen-bonded ammonia clusters, however, a bimodal velocity distribution of the ammonia monomer fragments has been observed recently [5].

The internal energy distribution of clusters and cluster fragments yields important information for the understanding of the microscopic dynamics in cluster-surface scattering. This degree of freedom has, however, largely been neglected in experimental and theoretical studies. In the pioneering work on nitrogen cluster scattering from metal surfaces Holland *et al.* [1] reported rotational distributions of N_2 monomer fragments obtained from electron beam induced fluorescence. Recently, Någård and Pettersson [9] derived from the temperature dependent fragmentation pattern of ethanol in a quadrupole mass spectrometer the internal energy of monomer fragments from ethanol clusters scattered off graphite. Using $(2+1)$ REMPI De Martino *et al.* [17] studied the dependence of the rotational distribution of N_2 fragments from nitrogen clusters scattered off graphite on the scattering angle and the surface temperature. They found a cold (~ 75 K) and a hot (~ 375 K) component which displayed the same temperatures at all scattering angles. The relative fraction of the cold component, however, significantly increased from about 10–20% to 50–60% when the detection angle was increased from $\vartheta_f = 30°$ to 80°. Extending the information

[a] *Present address*: CWW-Gerko Akustik, 67547 Worms, Germany.

[b] e-mail: hzach@nwz.uni-muenster.de

about internal energies to the primary subject we present in this paper results for the internal energy distribution of ammonia clusters in the incident beam and of small clusters scattered off a LiF(100) surface.

2 Experimental

Ammonia clusters are detected by single photon photoionization with vacuum ultraviolet (VUV) laser radiation tunable between $\lambda = 142.5$ nm ($h\nu = 8.7$ eV) and $\lambda = 126.5$ nm ($h\nu = 9.8$ eV). The VUV laser radiation is generated by two-photon resonant difference frequency mixing in Kr [17]. Frequency doubled radiation ($\lambda_{\rm uv} = 212.55$ nm) of a dye laser (Spectra Physics, PDL 3) pumped by the third harmonic of a seeded Nd:YAG laser (Spectra Physics, GCR 230) is tuned to the $(5p[1/2,0] \leftarrow 4p)$ two-photon resonance in krypton. This UV radiation is focussed ($f = 560$ mm) into a cell containing pure Kr at a pressure of about 10 mbar. The tunable output of an optical parametric oscillator (OPO) (GWU, type A) is directed into the conversion cell and overlaps with the UV laser radiation. This OPO is also pumped by part of the third harmonic of the same Nd:YAG laser. Using the signal beam of the OPO, tuned between $\lambda = 418.8$ nm ($h\nu = 2.96$ eV) and $\lambda = 666.6$ nm ($h\nu = 1.86$ eV), yields VUV laser radiation tunable between $\lambda_{\rm vuv} = 142.5$ nm and 126.5 nm. The spectral width of the resulting VUV laser radiation is determined by that of the OPO signal wave which varies between $\Delta\lambda = 2.5$ nm at about 650 nm and 0.25 nm at 425 nm. Thus, the spectral width of the generated VUV radiation varies between about $\Delta\tilde{\nu} = 15$ cm^{-1} ($h\Delta\nu \sim 2$ meV) at 142 nm and $\Delta\tilde{\nu} = 57$ cm^{-1} ($h\Delta\nu \sim 7$ meV) at 126 nm. In the entire tuning range the third-order susceptibility of the krypton gas is nearly constant [18]. Thus upon tuning the optimum pressure does not change and the generated VUV intensity remains nearly constant. Figure 1 shows the VUV output intensity for a single mirror set of the OPO in the range from 130.5 nm to 140 nm. Shorter and longer VUV wavelengths are covered by a "red" and a "blue" mirror set of the OPO.

The resulting VUV laser radiation is separated from both fundamental beams by a 30° LiF prism and focused into the ultrahigh vacuum (UHV) interaction chamber with a LiF lens ($r = 130$ mm). The VUV beam can enter the interaction chamber at two different levels. Inserting under vacuum two parallel aluminium mirrors into the beam path the VUV beam crosses the incoming supersonic molecular beam at right angle. The direct VUV beam traverses the interaction chamber 25 mm above the molecular beam in order to ionize the scattered particles. For all scattering events described here the clusters impinge on the LiF(100) surface at $\vartheta_{\rm i} = 45°$ while the scattered fragments are detected at an exit angle of $\vartheta_{\rm f} = 65°$. Since the velocity distributions of scattered fragments show their maximum at an exit speed of about 500 ms^{-1} [5] scattered particles with this velocity are selected in the present study. The experimental setup used for the scattering of neutral ammonia clusters off LiF(100) has been described

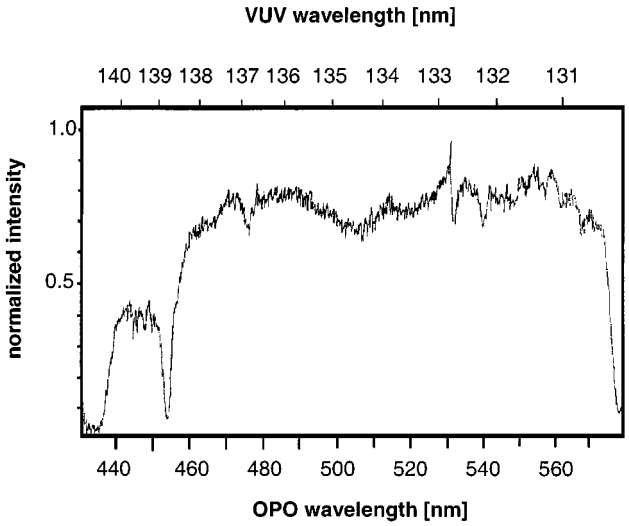

Fig. 1. Normalized VUV intensity for the signal output of the OPO using the "green" mirror set. For visible wavelengths below about 455 nm and above about 578 nm the OPO signal wave is produced by the "blue" and "red" mirror set, respectively. The signal output power is about the same for all three mirror sets.

in detail earlier [4,5]. Ammonia clusters are produced in the expansion of a 1:3 mixture of NH_3 and He through a 0.5 mm diameter and 5 mm long nozzle into the vacuum. The stagnation pressure of the mixture was 4 bar. Clusters of different size are produced in this supersonic molecular beam with the same mean kinetic energy of $\langle E_{\rm kin}\rangle = 285$ meV per ammonia molecule and an energy spread of $\Delta E_{\rm kin} = 32$ meV [5].

In order to normalize the measured intensity of each mass signal the intensity of the ionizing VUV beam is monitored by a vacuum photodiode (ITL, TF 1850) with a CsI cathode and a MgF_2 window. This photodiode is mounted outside the UHV chamber. The space between the LiF exit window of the vacuum chamber and the MgF_2 entry window of the photodiode is purged with nitrogen. In addition we used a tracing technique to record the photoionization efficiency (PIE) spectra of ammonia cluster ions. The gas mixture of NH_3 and He is doped with about 625 ppm of *m*-xylene by using a partial pressure of 2.5 mbar *m*-xylene in the 4 bar expansion. This concentration showed to be low enough to avoid the creation of *m*-xylene or mixed clusters and high enough to yield an intensity of the *m*-xylene monomer comparable to that of the ammonia cluster ions. For each spectrum the intensities of the detected clusters are normalized to the intensity of the detected *m*-xylene ions. The PIE curve of *m*-xylene is measured separately using the photodiode to normalize the VUV laser intensity, corrected for the effective transmission of the LiF exit and the MgF_2 entrance window of the photocathode tube. The PIE spectrum of *m*-xylene in the cluster beam is shown in Figure 2 together with earlier results from a gas phase measurement [19]. Both curves are normalized to one another at 9.8 eV. There are significant differences between the two measurements with the

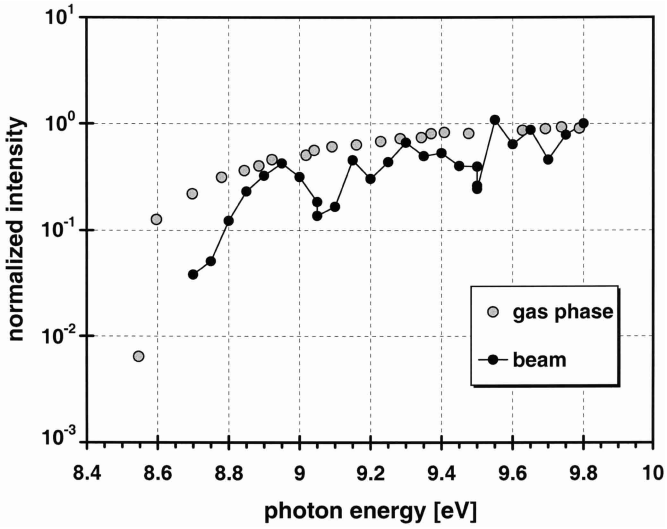

Fig. 2. Comparison between PIE spectra of *m*-xylene in the gas phase at room temperature (open circles) taken from reference [19] and in the seeded molecular beam (filled circles) obtained with the present experimental setup.

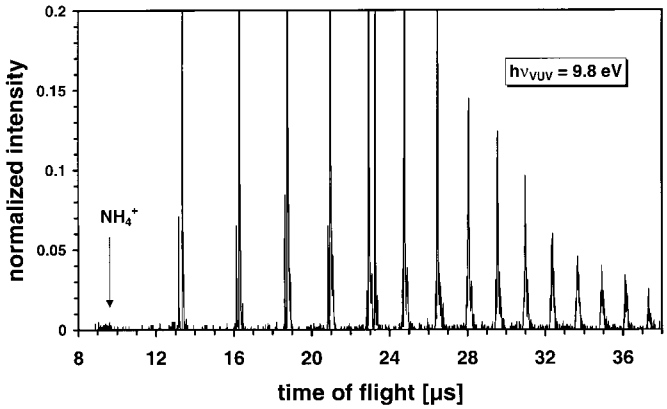

Fig. 3. Time-of-flight mass spectrum of ammonia clusters in the incident supersonic beam obtained at a photoionization energy of $h\nu = 9.8$ eV. The intensity scale is normalized to one for $(NH_3)_3NH_4^+$ ions which appear at about 18.8 μs. The expected position of NH_4^+ ions is marked by an arrow.

beam results showing a pronounced structure in the PIE curve of *m*-xylene.

3 Results

Figure 3 shows a typical TOF mass spectrum of the incident supersonic cluster beam, in this case obtained at a photon energy of $h\nu = 9.8$ eV. The intensity scale is enlarged by a factor of ten, and arbitrarily normalized to one at the mass of $(NH_3)_3NH_4^+$. Starting with $(NH_3)_2^+$ at a flight time in the reflectron of about 13 μs homogeneous and protonated cluster ions are observed, and shown in the figure up to $n = 16$. Remarkably, NH_4^+ ions are virtually not observed, which are expected to appear at a flight time of 9.6 μs, despite a recent literature value for

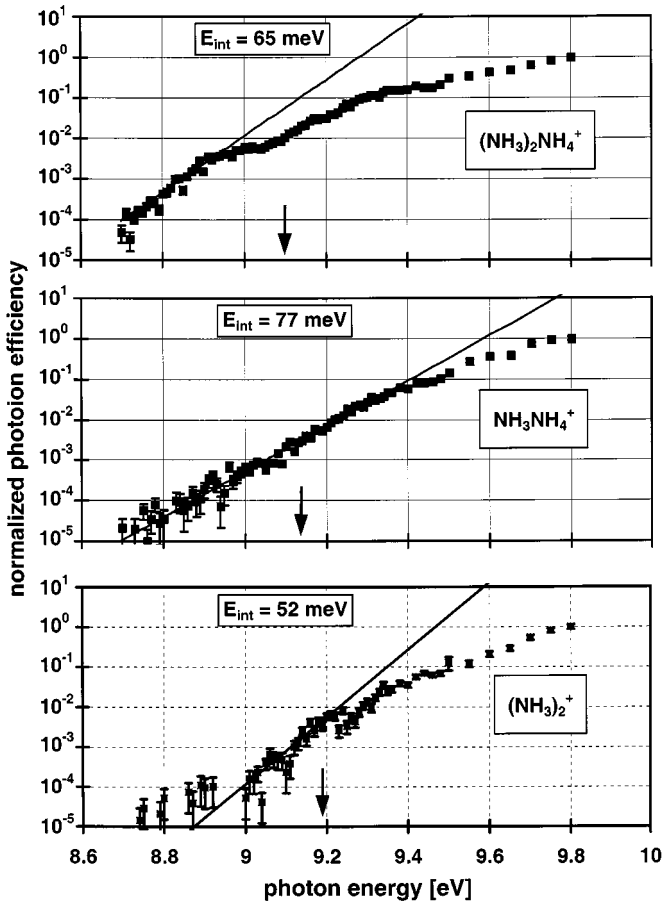

Fig. 4. PIE spectra (solid squares) of three small neutral clusters in the molecular beam. For data below the ionization potential, which is taken from reference [20] and marked with an arrow in each panel, the solid lines show the results of an exponential fit. The values for the internal energies obtained from these fits are indicated in each panel and are summarized in Table 1.

the appearance potential of 9.54 eV [20]. The signal at the NH_4^+ position is lower by at least a factor of 200 compared to that of $(NH_3)_3NH_4^+$. For ionizing radiation with $h\nu = 10.5$ eV photon energy ($\lambda = 118$ nm) the intensity of the NH_4^+ signal amounts to about 18% of the $(NH_3)_3NH_4^+$ signal for the same expansion conditions [4,5].

In Figure 4 are shown in a semi-logarithmic plot typical photoionization efficiency curves for small ammonia clusters in the incident supersonic beam, in particular for the homogeneous $(NH_3)_2^+$ and for clusters detected as protonated $NH_3NH_4^+$ and $(NH_3)_2NH_4^+$. It should be noted that the protonization reaction occurs only after the absorption of the VUV photon by the neutral cluster. This protonization is accompanied by the ejection of a NH_2 radical. Molecules measured as $(NH_3)_nNH_4^+$ in the reflectron thus originate from neutral $(NH_3)_{n+2}$ clusters [25]. The photoionization efficiency curves obtained for the protonated clusters thus reflect the ionization of the corresponding neutral clusters. In all cases the PIE curves display over up to five orders of magnitude a smooth and at low photon

Table 1. Average internal energies $E_{\rm int}$ of neutral clusters in the incident seeded supersonic beam. (The homogeneous cluster ions $(NH_3)_n^+$ origin from neutral $(NH_3)_n$ clusters of the same size, protonated $(NH_3)_{n-2}NH_4^+$ origin also from neutral $(NH_3)_n$ clusters.)

Cluster, measured as	$E_{\rm int}$ [meV]	$T_{\rm cluster}$ [K]
NH_4^+	–	–
$(NH_3)_2^+$	52	28
$NH_3NH_4^+$	77	27
$(NH_3)_3^+$	80	28
$(NH_3)_2NH_4^+$	65	17
$(NH_3)_4^+$	48	12
$(NH_3)_3NH_4^+$	52	10
$(NH_3)_5^+$	50	10
$(NH_3)_4NH_4^+$	51	9
$(NH_3)_6^+$	44	7
$(NH_3)_5NH_4^+$	52	7
$(NH_3)_7^+$	58	8
$(NH_3)_6NH_4^+$	66	8
$(NH_3)_8^+$	76	9
$(NH_3)_7NH_4^+$	67	7
$(NH_3)_9^+$	57	6
$(NH_3)_8NH_4^+$	68	7
$(NH_3)_{10}^+$	75	7
$(NH_3)_9NH_4^+$	67	6
$(NH_3)_{11}^+$	83	7
$(NH_3)_{10}NH_4^+$	76	6
$(NH_3)_{12}^+$	76	6
$(NH_3)_{11}NH_4^+$	81	6
$(NH_3)_{12}NH_4^+$	76	5
$(NH_3)_{13}NH_4^+$	71	5

energies an exponential increase with increasing photon energies. The only exception being the ammonia dimer, where between $h\nu = 8.7$ and 9.3 eV deviations from an exponential rise is observed, which may possibly be caused by the internal vibrational structure of this molecule. The sensitivity of the experiment does, however, presently not permit a definite assignment of this structure to specific vibrational modes. In each panel a recent literature value [20] of the appearance potential is indicated by an arrow. At photon energies below this value the PIE spectrum is fitted with an exponential Boltzmann distribution. The mean internal energies of the clusters derived from such fits are summarized in Table 1 for dimer to $n = 15$ clusters together with their protonated companions. It can be noticed that the internal energies of the detected cluster ions do not vary significantly with cluster size. Pairs of homogeneous and protonated detected cluster ions, like $(NH_3)_5^+$ and $(NH_3)_3NH_4^+$, which nominally origin from the same neutral cluster, show about the same internal energy. When all internal energies of all clusters measured

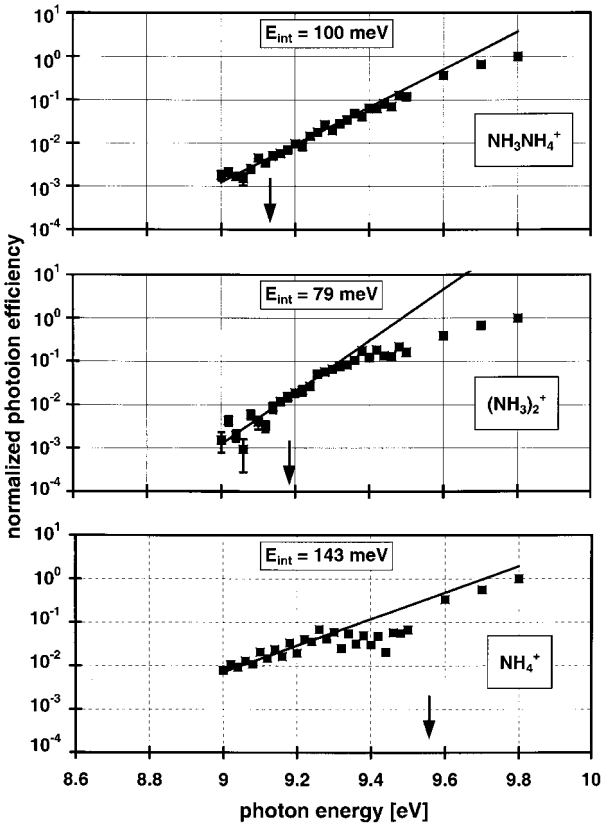

Fig. 5. Same as Figure 4, but for neutral cluster fragments scattered off the LiF(100) surface ($\vartheta_{\rm i} = 45°$, $\vartheta_{\rm f} = 65°$). The flight time of neutral clusters between the surface and the ionizing laser beam was 50 μs. The low signal-to-noise ratio due to the low particle density in the scattered flux did not permit to obtain data at photon energies below 9.0 eV.

are averaged one arrives at $\langle E_{\rm int}\rangle = (65 \pm 3)$ meV. A cluster temperature can be derived when the measured internal energy is divided by the number of internal degrees of freedom, $3n-3$. For the detected protonated clusters the ejection of a NH_2 radical upon ionization has to be accounted for by increasing the degrees of freedom by nine when the temperature of the originally neutral cluster is determined. Again, the temperatures of the neutrals derived from pairs of homogeneous and the protonated cluster ions are very similar. These temperatures decrease with increasing cluster size down to about 5–6 K, for the expansion conditions of the present experiment.

Figure 5 shows PIE spectra for three different cluster fragments, NH_4^+, $(NH_3)_2^+$ and $NH_3NH_4^+$, scattered off LiF(100). Due to the lower particle density in the scattered flux measurements of the PIE could not be obtained with sufficient signal-to-noise ratio for photon energies below $h\nu = 9.0$ eV. Again the internal energy is obtained from a Boltzmann fit to the data points at photon energies between $h\nu = 9.0$ and 9.3 eV. Table 2 lists the results for all scattered cluster fragments observed. The internal cluster temperatures $T_{\rm cluster}$ are obtained in the same way as for incident clusters and are listed also in Table 2. It should be noted that in the scattered flux NH_4^+

Table 2. Average internal energies of neutral clusters scattered off LiF(100).

Cluster, measured as	E_{int} [meV]	T_{cluster} [K]
NH_4^+	143	79
$(NH_3)_2^+$	79	40
$NH_3NH_4^+$	100	37
$(NH_3)_2NH_4^+$	142	37

ions could now be detected in the photon energy range from 9.0 to 9.8 eV. The internal energy of this species amounts to about $E_{\mathrm{int}} = 143$ meV. For larger clusters the internal temperature is about 37 K and does not change much with cluster size. This translates into an increasing internal energy with increasing cluster size, as far as the limited data set suggests.

4 Discussion

The central result for clusters in the incident beam is the approximately constant internal energy of about 65 meV. This correlates with a constant velocity of all clusters in this beam which was observed in an earlier experiment [5]. Both features suggest that the clusters are formed in an early part of the expansion, and after formation still exchange energy and momentum with the He carrier gas. For larger clusters the final cluster temperature decreases since the floppier intermolecular vibrations in larger clusters can be cooled more effectively in the propagating expansion. This phenomenon has been earlier observed in the expansion of various monomers [21]. It should be kept in mind, however, that our analysis is based on the assumption of a constant Franck-Condon factor for the ionization of various internal vibrations of a specific cluster. On the other hand this assumption is supported by the single exponential decrease of the photoionization yield with decreasing photon energy.

The missing observation of NH_4^+ at photon energies up to 9.8 eV is in contrast to earlier photoionization measurements, which derived appearance potentials of 9.59 eV [22] and 9.54 eV [20]. It is, however, in accord with the results of a study using electron impact ionization. There an appearance potential of 9.95 eV was reported [23]. In both photoionization experiments PIE curves of ammonia clusters from expansions of neat ammonia were recorded, whereas in the electron impact study as well as in the present work ammonia clusters were formed in the presence of excess He carrier gas. It thus might cautiously be concluded that the results of the earlier photoionization studies were derived from ammonia clusters with considerable internal energy.

The internal energies of cluster fragments scattered off LiF(100) are higher than in the incident beam, but lower than might be expected for clusters arriving at the surface with a normal kinetic energy of about $E_{\mathrm{kin},\perp} = 200$ meV per monomer constituent. However, the internal energy measured represents the remaining part of the initial internal energy of scattered clusters detected after a flight time of about 50 μs between the scattering event and the ionizing laser pulse. This long time favors the process of evaporative cooling [24] while the fragments are leaving the surface. Thus the detected internal energy is that part which is not sufficient to desorb another ammonia monomer from the cluster. Due to statistical reasons the mean energy remaining in the cluster fragments then should be of the order of half the monomer binding energy for the given cluster size. The values listed in Table 2 are in accord with this estimation.

Even the comparatively high value for NH_4^+ together with the low internal energy of $(NH_3)_2^+$ can be explained this way. Taking into account that no NH_4^+ could be detected in the molecular beam at the same experimental conditions, the NH_4^+ ions detected in the scattering flux must origin from those dimers or larger fragments scattered off the surface which carry a large amount of internal energy. On the other hand the detected homogeneous dimer ions $(NH_3)_2^+$ have been neutral dimers before absorbing the ionizing photon. Due to the exothermic nature of the internal proton transfer reaction hindered only by a small activation barrier of about 100 meV [25] the probability for detecting a $(NH_3)_2^+$ ion is only significant for neutral dimers with low internal energy. Highly excited neutral dimers are favored to be detected as NH_4^+ ions. Thus, for an ensemble of scattered neutral ammonia dimers with a given internal energy the PIE spectrum of the detected NH_4^+ ions is expected to show a higher internal energy than the PIE spectrum of $(NH_3)_2^+$ ions.

In molecular cluster scattering internal energies have only recently been reported by Någård and Pettersson [9] for evaporated ethanol monomers from ethanol clusters and by De Martino *et al.* [17] for N_2 from nitrogen clusters impinging on graphite surfaces. The internal temperature of ethanol was determined from the temperature dependent fragmentation pattern in a quadrupole mass spectrometer. Up to a surface temperature T_{s} of about 550 K the internal temperature of ethanol was accommodated to the surface, but at higher T_{s} up to 1 400 K it leveled off at about 600 K. This behaviour resembles that of monomer scattering from various surfaces [26]. These temperatures are significantly higher than those reported in this work for the remaining internal energy of surviving cluster fragments. In the case of N_2 the rotational population distribution was determined by $(2+1)$ REMPI. A bimodal distribution which can be described by rotational temperatures of $T_{\mathrm{rot}} = 75$ K and 375 K was found. While these temperatures did not vary systematically with the scattering angle, the fraction of the cold distribution increased significantly when the scattering angle increased from $\vartheta_{\mathrm{f}} = 30$ to 80° [17]. The internal energies of ammonia clusters scattered off LiF(100) are probably reduced by evaporative cooling to the low values observed in this study. This conjecture is supported by the fact that only a few, small clusters are observed after scattering. For more elucidating information the flight time of clusters between the scattering event and the detection should be significantly reduced. Meanwhile, investigations of the internal

energy of evaporated NH_3 monomers, which can be determined with internal state selectivity *via* $(2 + 1)$ REMPI, may thus yield more direct information about the dynamic processes during cluster scattering.

The authors gratefully acknowledge the financial support by the Deutsche Forschungsgemeinschaft in the Schwerpunktprogramm "Molekulare Cluster" under project number Za 110/10.

References

1. R.J. Holland, G.Q. Xu, J. Levkoff, A. Robertson Jr, S.L. Bernasek, J. Chem. Phys. **88**, 7952 (1988).
2. M. Châtelet, A. De Martino, J. Pettersson, F. Pradère, H. Vach, Chem. Phys. Lett. **196**, 563 (1992).
3. H. Vach, A. De Martino, M. Benslimane, M. Châtelet, F. Pradère, J. Chem. Phys. **100**, 8526 (1994).
4. C. Menzel, A. Knöner, J. Kutzner, H. Zacharias, Z. Phys. D **38**, 179 (1996).
5. C. Menzel, R. Baumfalk, H. Zacharias, Chem. Phys. **239**, 287 (1998).
6. A.A. Vostrikov, A.M. Zadorozhny, D.Yu. Dubov, G. Witt, I.V. Kazakova, O.A. Bragin, V.G. Kazakov, V.N. Kikhtenko, A.A. Tyutin, Z. Phys. D **40**, 542 (1997).
7. P.U. Andersson, J.B.C. Pettersson, Z. Phys. D **41**, 57 (1997).
8. P.U. Andersson, A. Tomsic, M.B. Andersson, J.B.C. Pettersson, Chem. Phys. Lett. **279**, 100 (1997).
9. M.B. Någård, J.B.C. Pettersson, Chem. Phys. Lett. **293**, 535 (1998).
10. G.Q. Xu, S.L. Bernasek, J.C. Tully, J. Chem. Phys. **88**, 3376 (1988).
11. G.Q. Xu, R.J. Holland, S.L. Bernasek, J.C. Tully, J. Chem. Phys. **90**, 3831 (1989).
12. J.B.C. Pettersson, N. Markovic, Chem. Phys. Lett. **201**, 421 (1993).
13. N. Markovic, J.B.C. Pettersson, J. Chem. Phys. **100**, 3911 (1994).
14. M. Svanberg, N. Markovic, J.B.C. Pettersson, Chem. Phys. **220**, 137 (1997).
15. M. Svanberg, N. Markovic, J.B.C. Pettersson, Chem. Phys. **201**, 473 (1995).
16. H. Vach, M. Benslimane, M. Châtelet, A. De Martino, F. Pradère, J. Chem. Phys. **103**, 1972 (1995).
17. A. de Martino, M. Châtelet, F. Pradère, E. Fort, H. Vach, J. Chem. Phys. **111**, 7038 (1999).
18. R. Brünger, thesis, Hannover, 1992.
19. M.E. Akopyan, F.I. Vilesov, Russ. J. Phys. Chem. **40**, 63 (1966).
20. W. Kamke, R. Herrmann, Z. Wang, I.V. Hertel, Z. Phys. D **10**, 491 (1988).
21. *Atomic and Molecular Beam Methods*, edited by G. Scoles (Oxford University Press, 1988).
22. S.T. Ceyer, P.W. Tiedemann, B.H. Mahan, Y.T. Lee, J. Chem. Phys. **70**, 14 (1979).
23. K. Stephan, J.H. Futrell, K.I. Peterson, A.W. Castleman Jr, H.E. Wagner, N. Djuric, T.D. Märk, Int. J. Mass Spectrom. Ion Phys. **44**, 167 (1982).
24. E. Kaiser, J. de Vries, H. Steger, C. Menzel, W. Kamke, I.V. Hertel, Z. Phys. D **20**, 193 (1991).
25. J.C. Greer, R. Ahlrichs, I.V. Hertel, Z. Phys. D **18**, 413 (1991).
26. H. Zacharias, Int. J. Mod. Phys. B **4**, 45 (1990).